XLVI CILAMCE
VITÓRIA - ES - BRAZIL - 2025
XLVI IBERO-LATIN AMERICAN CONGRESS ON COMPUTATIONAL METHODS IN ENGENEERING

A continuous projection-based embedded discrete fracture model for the numerical simulation of groundwater contaminant transport using 2D unstructured meshes

Emanoel Rodrigues dos Santos[1], Pedro Victor Paixão Albuquerque[1], Gabriel Martins Cavalcanti Feitosa[2], Fernando Raul Licapa Contreras[1], Artur Castiel Reis de Souza[3],Paulo Roberto Maciel Lyra[1] , Darlan Karlo Elisário de Carvalho[1].

[1]*Department. of Civil Engineering, UFPE*
Rua Acadêmico Hélio Ramos s/n, Cidade Universitária. CEP 50.740-530, Recife, PE, Brazil
emanoel.rsantos@ufpe.br, paixao.albuquerque@ufpe.br, fernando.raul@ufpe.br, darlan.ecarvalho@ufpe.br, Universidade Federal de Pernambuco.
[2]*Department. of Mechanical Engineering, UFPE*
Av. da Arquitetura s/n, 2° Andar do Bloco Escolar. CEP 50740-550, Recife, PE, Brazil
gabriel.gmcf@ufpe.br
[2]*Faculty of Civil Engineering and Geosciences, TUDelft.*
Building 23 Stevinweg 1 2628 CN Delft, the Netherlands
artur.castiel@tno.nl

Abstract. The pollution of groundwater stored in aquifers can pose serious risks to human health and also harm the ecological environment. In many geological settings, aquifers are located within naturally fractured reservoirs (NFRs)—rock formations that contain fractures which can function either as a high permeable conduit or as a barrier. These fractures arise from geological processes and exhibit diverse properties, increasing the complexity of building accurate simulation tools. The development of robust and accurate computational models is of utmost importance to understand the processes of contaminant transport in aquifers. In this work, we propose a new variant of the Continuous Projection-based Embedded Discrete Fracture Model (CpEDFM) to model fractures in 2D domains. The method maps the nodes of the cells that contain embedded fractures onto a graph, where the edges between graph nodes correspond to control surfaces. A pathfinding algorithm is applied to determine the shortest path between the nodes representing the fracture endpoints. This path is subsequently projected back onto the reservoir grid, selecting the cell faces that will receive the fracture projections while ensuring projection continuity. We evaluate the performance of the proposed CpEDFM algorithm by solving benchmark of the fluid flow subproblems found in literature.

Keywords: Contaminant transport simulation, Numerical groundwater modeling, Naturally fractured reservoir, Embedded Discrete Fracture Model.

1 Introduction

One of the primary challenges in the characterization of fractured aquifers is the complexity due to its anisotropic and heterogeneity formations. In the last decades, researchers created models to improve the characterization of different fractures [1], each aiming to represent the hydraulic behavior of fractures while maintaining the computational efficiency. One of the first approach was the dual-continuum model.While computationally efficient, dual-continuum models rely heavily on upscaling and assume idealized fracture-matrix interactions, limiting their accuracy in highly heterogeneous systems. To characterize the fractures explicitly, the Discrete Fracture Model (DFM) was introduced for simulating NFRs. In DFM, fractures are modeled as separate entities within the matrix, typically with lower dimensionality, allowing more detailed simulation of flow along fractures. On the other hand, the DFM uses unstructured conforming meshes to fractures, increasing its computational cost [2]. To overcome the mesh conforming limitation in DFM models, the Embedded Discrete Fracture Model, introduced by [3] and further expanded on by [4], arrived as the most effective and precise model for simulating fracture networks . In this method, two different meshes are used for the matrix and fractures domains, in which fractures are explicitly considered. In the EDFM, the fluid flow within the matrix - fracture or fracture - fracture domains is proportional to

the pressure difference between them, without conforming meshes. Although, recent studies exhibited an inability to deal with very low permeability fractures (flow barriers)[5] and to model the early transient fluid flow near fractures accurately [2][6]. In 2017, a modified EDFM was created, the projection-based Embedded Discrete Fracture Model (pEDFM) builds additional connections between the fracture cells and the cells surrounding the matrix cell containing the fracture [5]. These additional Non-Neighbour Connections (NNCs) in pEDFM model are achieved by projecting the fracture length onto matrix cells faces, improving the simulation of NFRs accuracy considering fractures with a wide range of permeabilities. Nevertheless, in specific cases the projection algorithm present in pEDFM may lead to discontinuities through which the fluid can flow [7].The preliminary results presented in section 4 shows the importance of a continuous projection of fractures in single-phase problems. Furthermore, the version that incorporates contaminant transport is in the final verification phase. A cell-centered Finite Volume Method (FVM) is used to discretize both matrix and fractures domain, the system of equations, considering the transport problem, is solved by a segregated IMPEC (Implicity Pressure, Explicit Concentration) algorithm. In addition, the dispersion term and the Darcy's diffusive flux are discretized by the Multipoint Flux Approximation with Diamond stencil (MPFA-D) [8][9] while in the fracture - including NNC, the MPFA-D becames a Two-Point Flux Approximation (TPFA), due to the fracture structured meshes. The linearity-preserving interpolation with explicit weights (LPEW2) [8] is used to the MPFA-D nodal interpolation and the advective term in both domains is discretized using a high-order MUSCL-type FVM. Finally, a Multidimensional Limiting Process (MLP) [10] is used to avoid numerical oscillations.

2 Mathematical Model

In this section, the governing equations of the mathematical model for isothermal, miscible, and incompressible contaminant transport in naturally fractured porous media are presented[11]. Considering a 2D matrix Ω_m domain containing embedded fractures Ω_{f_k}, where the m index represents the terms related to the rock matrix and those related to the $k-$th fractures within the domain are represented by f_k. Considering the fracture domain as $n-1$ dimensional, the concentration field $c(x,t)$, without considering the gravitational term is given by[10]:

$$\phi\frac{\partial}{\partial t}(c)_m + \nabla.(c\vec{v})_m + \nabla.(-\mathbf{D}\nabla c)_m = (q)_m + \sum_{k=1}^{n_{frac}} (\Psi)_{m,f_k}, \tag{1}$$

where ϕ, c, n_{frac} and q represents the medium porosity, the solute concentration, the number of fractures within the domain Ω_m and source/sink terms, respectively. The velocity v is given by Darcy's law $v = -\lambda\mathbf{K}\nabla p$ where λ is the mobility, $\nabla.(-\mathbf{D}\nabla c)$ represents the molecular diffusion term, given by Fick's law, $\mathbf{K}$ is the rock absolute permeability tensor and p is the fluid pressure. Furthermore, we can write the following expression for the mass transfer term between Ω_m and Ω_{f_k} and between different fractures Ω_{f_k}, Ω_{f_j}[12]:

$$(\Psi)_{m,f_k} = \mathbf{K}_{m,f_k}\frac{CI^{m,f_k}}{A_m}(p^m - p^f) \ \ , \ \text{ and } \ (\Psi)_{f_k,f_j} = \mathbf{K}_{f_k,f_j}\frac{CI^{f_k,f_j}}{A_{f_k}}(p^{f_k} - p^{f_j}) \ \ , CI = \frac{S_{k,j}}{d_{k,j}}. \tag{2}$$

in both equations, (2), CI is the connectivity index, (where S is the embedded fracture segment length and d is the average distance of matrix/fracture cell and the respective fracture segment), A_m and A_{f_k} denotes the area of a matrix cell intersected by fracture and the area of fracture cells intersecting each other, respectively. Similarly to (1), the transport equation for the $k-$th fracture domain Ω_{f_k} can be written:

$$\varpi\phi\frac{\partial}{\partial t}(c)_{f_k} + \varpi\nabla.(c\vec{v})_{f_k} + \varpi\nabla.(-\mathbf{D}\nabla c)_{f_k} = (q)_{f_k} + (\Psi)_{m,f_k} + \sum_{j=1}^{n_{frac}} (\Psi)_{f_k,fj;j\neq k}, \tag{3}$$

where ϖ is the fracture aperture ,$(\Psi)_{m,f_k}$,$(\Psi)_{f_k,f_j}$ represents the mass transfer term between Ω_m and Ω_{f_k} and between Ω_{f_k} and Ω_{f_j}, respectively. It is important to note that the aquifer is completely saturated with water. The elliptic pressure equation for both domains Ω_m and Ω_{f_k} can be written:

$$\nabla(v) = (q)_m + \sum_{i=1}^{nfrac} (\Psi)_{m,f}, \ and \ \varpi\nabla(v) = (q)_{f_k} + \sum_{i=1}^{nfrac} (\Psi)_{m,f} + \sum_{j=1}^{nfrac} (\Psi)_{f_j,f_k,j\neq k}. \tag{4}$$

2.1 Boundary conditions

The contaminant transport problem can only be completely determined if the appropriate set of initial and boundary conditions such as:

$$\begin{aligned} p(x,t) &= p_D, \quad && \text{on} \quad \Gamma_m^D \times [0,t], \\ \vec{v}.\vec{n} &= \bar{g}_{p,N}, \quad && \text{on} \quad \Gamma_m^N \times [0,t], \\ -\mathbf{D}\nabla c \cdot \vec{n} &= \bar{g}_{c,N} \quad && \text{on} \quad \Gamma_m^c \times [0,t], \\ c(x,0) &= c_0, \quad && \text{on} \quad \Omega_m, t = 0, \end{aligned}$$

where Γ_m^D and Γ_m^N are the boundaries with Dirichlet and Neumann conditions, respectively. Furthermore, t is the time variable, p_D and c_D are the known scalar functions representing the pressure and concentration, while $\bar{g}_{p,N}$ is a known scalar function representing the flux. Additionally, $\vec{n}$ is the unit outward normal vector to the control surface, $c(x,0)$ is the initial solute concentration. Moreover, it is worth highlighting that all fractures are assumed to be entirely enclosed within Ω_m.

3 Numerical Formulation

This section describes the numerical formulation developed to simulate the transport problem in naturally fractured aquifers, using 2-D general meshes. The Multi-point Flux Approximation with Diamond stencil (MPFA-D) proposed by [8] is used to calculate the flux in the matrix domain, Ω_m while the Two-Point Flux Approximation (TPFA) evaluates the flux in the NNCs and fracture's domain Ω_{f_k} .

3.1 The Pressure Equation

By integrating the pressure equations eq. (4)

$$\int_{\Gamma_i} v.N \, d\Gamma_i = \int_{\Omega_i} Q \, d\Omega_i + \int_{\Omega_i} \sum_{i=1}^{nfrac} (\Psi)_{m,f} \, d\Omega_i \rightarrow \sum_{IJ \in \Gamma_i} V_{IJ}.N_{IJ} = \bar{Q}_{\Omega i} + \sum_{i=1}^{nfrac} (\Phi)_{m,f}, \tag{5}$$

where IJ are nodes of a generic cell, Γ_i represents the external edges, $\bar{Q}$ is the average source/sink term, V_{IJ} is the face average flux and $N_{IJ} = |e|.\vec{n}$ is the product of the face length $|e|$ and the unitary outward normal vector of the face and $(\Phi)_{m,f} = \int_{A_{m,f}} \sum_{i=1}^{nfrac} (\Psi)_{m,f} \; dA_{m,f}$. The same procedure is used to discretize the equation (**??**) in fractures domain Ω_{f_k}, with $(\Phi)_{f_j,f_k} = \int_{l_{j,k}} \sum_{m=1}^{nfrac} (\Psi)_{j,k} \; dl_{j,k}$:

$$\begin{aligned} \varpi \int_{\Gamma_i} v.N \, d\Gamma_i = \int_{\Omega_i} Q \, d\Omega_i + \int_{\Omega_i} (\Psi)_{m,f} \; + \int_{\Omega_{f_i}} \sum_{j=1}^{nfrac} (\Psi)_{f_j,f_k,j \neq k} \, d\Omega_{f_i} \rightarrow \\ \sum_{IJ \in \Gamma_i} V_{IJ}.N_{IJ} = \bar{Q}_{\Omega i} + (\Phi)_{m,f} \; + \sum_{j=1}^{nfrac} (\Phi)_{j,k,j \neq k}, \end{aligned} \tag{6}$$

3.2 Continuous projection-based Embedded Discrete Fracture Model

Similar to the standard EDFM approach, pEDFM treats fractures as lower-dimensional-entities—lines in 2D within the matrix mesh. Nevertheless, the conventional EDFM method may face challenges in accurately modeling cases with low permeability fractures [13]. To overcome these limitations, pEDFM introduces a projection technique to compute the flux exchange between fractures and the surrounding matrix. Specifically, the method projects the fracture surface onto the normal direction of the intersected matrix cells. This projection-based approach improves the estimation of matrix-fracture and fracture-fracture fluxes. However, recent studies [7] have

identified discontinuities in the projection algorithm employed by the pEDFM, which can lead to inaccuracies, particularly in scenarios involving low-permeability fractures [6]. In this work, a new projection-based algorithm is proposed to accurately model different fracture networks, with a wide range of permeabilities, including flow barriers. Figure 1 illustrates the additional Non-Neighboring Connections (NNCs) introduced by the pEDFM [14], in comparison to the standard EDFM. These additional connections are generated by projecting the fracture segments onto the faces of the matrix cells. The projection algorithm is used to identify the cells within fractures and to construct the graph using the cell nodes. Finally, the Dijkstra's algorithm is used to find the shortest path , posteriorly used as fracture projection.

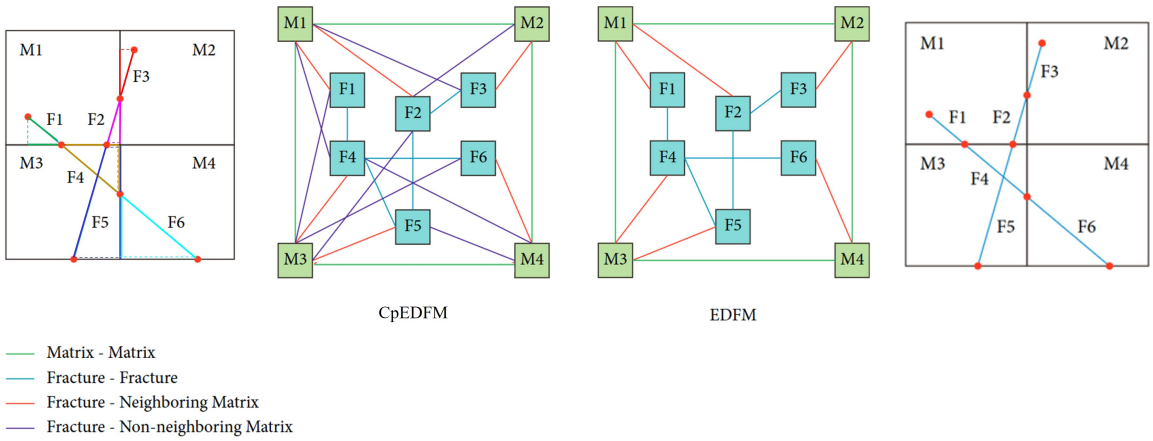
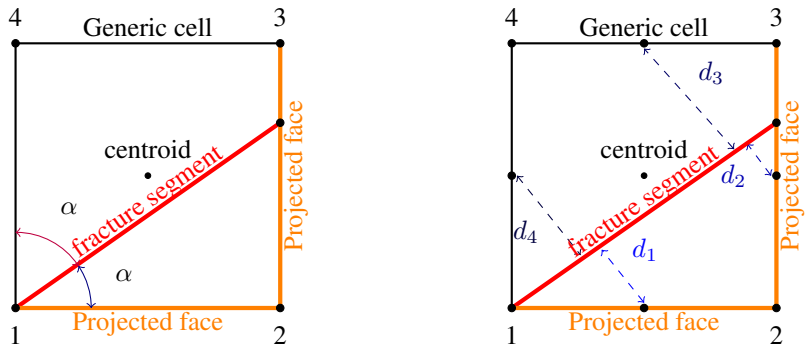


Figure 1. Fracture segments and their Non-Neighbor Connections in pEDFM and standard EDFM, respectively.

3.3 The Projection algorithm



Remark: Both criteria shown above can be used, without losing accuracy.
The algorithm developed to project fractures onto cell faces uses computational geometry and the concept of the graph to ensure the continuity of the projection. This algorithm is fundamental to define the Non-neighbour Connections, its use ensures that the fractures are correctly connected to matrix cells, allowing an accurate representation of the matrix-fracture connection. It begins by identifying the cells that intersect with the fractures. Once these cells are located, the next step ensures that at least one face of each selected cell is suitable for receiving the projected fracture. With the appropriate faces identified, a graph is constructed based on the nodes of these faces, effectively representing the connectivity between potential projection points. Finally, a pathfinding algorithm—specifically Dijkstra's algorithm [15]—is employed to determine the shortest path through this graph, ensuring an efficient and accurate projection of the fracture geometry onto the mesh.Two different criteria can be used to determine the weighting used to select which face will receive the projection. The first is based on the angle between the projection and the face, such that the smaller the angle between them, the greater the weighting for face selection. The second is based on the perpendicular distance between the fracture and the center of the matrix control volume, which the minor distance is used to define the face which will receive the projection.

4 Results

The accuracy and robustness of our CpEDFM is evaluated using some examples. The results were compared with the HMF model present in the Matlab Reservoir Simulation Toolbox (MRST), this model is an approach for fractured reservoirs that allows the simulation of explicitly represented fractures alongside a coarse-scale matrix. The first result considers a simple fracture network with two high-permeable fractures, the second is a single low-permeable fracture. The computational domain considered is a two-dimensional rectangular region with dimensions $[10 \times 5]$. The rectangle is defined by four corner nodes: node 1 at the bottom-left, node 2 at the bottom-right, node 3 at the top-right, and node 4 at the top-left. The boundary conditions applied to the domain are summarized as follows. Along the bottom edge (Boundary 1–2) and the top edge (Boundary 3–4), a no-flux condition is imposed, expressed as $v \cdot \vec{n} = 0$. On the right edge (Boundary 2–3), the pressure is prescribed as $p = 0$, while on the left edge (Boundary 4–1), a pressure boundary condition $p = 1$ is applied.

4.1 Error norm

In order to verify our methods, the pressure in each configuration is evaluated considering the infinity norm, which measures the largest absolute value in a vector or the maximum error between two vectors, returning the largest absolute value among the elements of the pressure vector.

$$\|P_{\text{num}} - P_{\text{ref}}\|_\infty = \max_{1 \le i \le n} |P_{\text{num},i} - P_{\text{ref},i}| \tag{7}$$

4.2 Result 1: A simple high-permeable fracture network

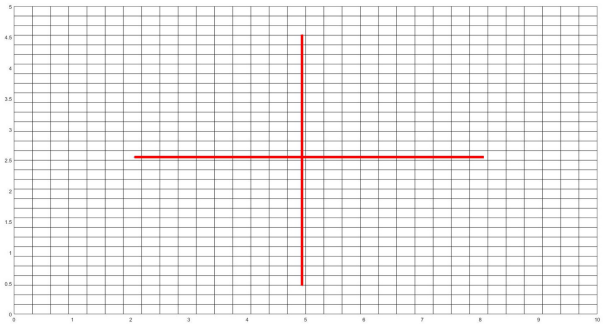


Figure 2. Computational mesh (4.096 matrix cells) with two high permeable fractures.

Table 1. General parameters.

Properties	Value	Units
Fracture Porosity	0.8	–
Fracture Permeability	$1,000$	m^2
Fracture Aperture	10^{-3}	m
Matrix Permeability	1	m^2

Table 2. Maximum pressure difference using different mesh resolutions.

	Mesh resolution				
N_{vc}	8x8	16x16	32x32	64x64	128x128
P_{diff}	$2.69 \cdot 10^{-13}$	$1.76 \cdot 10^{-13}$	$2.25 \cdot 10^{-13}$	$2.28 \cdot 10^{-11}$	$9.21 \cdot 10^{-11}$

Figure [3] displays the pressure isolines obtained (MRST and our CPEDFM) almost overlapping each other. The results in Table **2** present the pressure error obtained for each mesh resolution. As the number of control volumes increases from 8×8 to 128×128, it is possible to observe that the error remains on the order of 10^{-13} for coarser meshes, but increases slightly for finer resolutions.

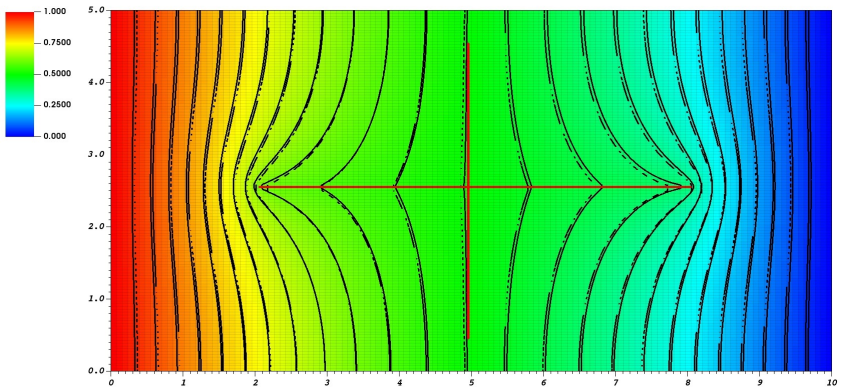
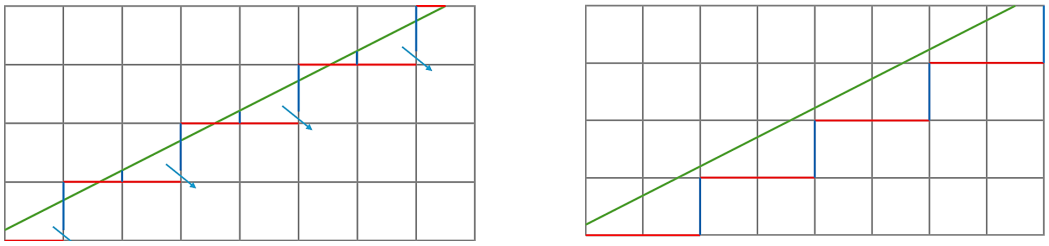


Figure 3. Porous media with double highly permeable fractures - Pressure field.

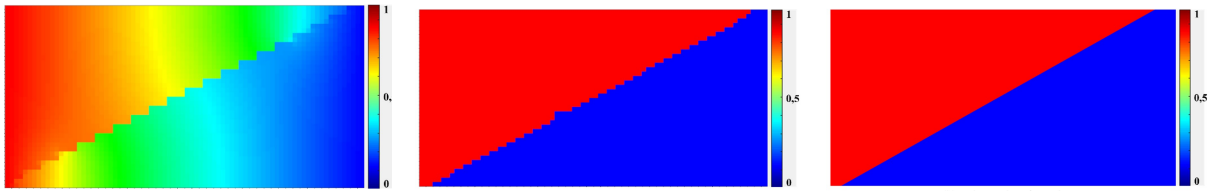
4.3 Result 2: A single barrier

Under the same boundary conditions and general properties, figure 4a presents the reservoir with a single inclined fracture with low permeability that crosses the entire domain. In this case, the projection algorithm select the faces that will receive the projection, modifying its transmissibilities and Non-Neighbour Connections. In addition, it is possible to note the existence of gaps (indicated by the arrow) 4a in pEDFM projection, allowing artificial fluid flow. On the other hand, by using the CpEDFM 4b it is possible to verify the continuous fracture projection. As result, the CpEDFM can provide more realistic simulations of fractures with a wide range of permeabilities.



(a) pEDFM fracture's projection (b) CpEDFM fracture's projection

Figure 4. Differences in projection algorithm. (a) pEDFM and (b) CpEDFM.



(a) pEDFM (b) CpEDFM (c) Reference solution

Figure 5. Comparison of pressure field for pEDFM, CpEDFM and the reference solution.

Figure 5 presents the pressure fields obtained for the previous case using the pEDFM 5a, CpEDFM 5b, and an equidimensional model with a highly refined mesh as reference solution (51.200 control volumes) 5c. The CpEDFM result shows excellent agreement with the reference solution, successfully capturing the expected pressure distribution throughout the domain. In contrast, the pEDFM solution exhibits noticeable discrepancies due to gaps in the projection algorithm, which compromise the overall accuracy.

5 Conclusions

In the present work, an alternative Continuous projection-based Embedded Discrete Fracture Model is proposed. As in the pEDFM, the additional Non-Neighboring connections between fracture cells and the non-

neighboring matrix cells present in CpEDFM achieve a more realistic representation of the flux across fracture networks. The transmissibility between the fracture control volumes and the adjacent matrix element, as well as the transmissibility between the fracture control volume and the additional non-adjacent matrix control volume, are computed independently using the cell faces length. The CpEDFM provided good results in terms of the pressure field when compared to benchmark results, which confirms the accuracy of the CpEDFM in modeling Naturally Fractured Reservoirs. In addition, we should remark that the CpEDFM formulation that have been tested for single phase flow is under extension to deal with the contaminant transport in naturally fractured porous media.

Acknowledgements.

The authors would like to thank PPGEC-UFPE, CNPq , FACEPE and CAPES for their financial support.

Authorship statement. The authors hereby confirm that they are the sole liable persons responsible for the authorship of this work, and that all material that has been herein included as part of the present paper is either the property (and authorship) of the authors, or has the permission of the owners to be included here.

References

[1] B. Van Riet, S. Six, K. Walraevens, A. Vandenbohede, and T. Hermans. Assessing the impact of fractured zones imaged by ert on groundwater model prediction: A case study in a chalk aquifer in voort. *Frontiers in Water*, 2021.

[2] S. Rostami, F. Boukadi, M. Bodaghi, and others. Review of embedded discrete fracture models: Concepts, simulation and pros & cons. *Petroleum & Petrochemical Engineering Journal*, vol. 7, n. 2, pp. 1–15, 2023.

[3] L. Li and S. H. Lee. Efficient field-scale simulation of black oil in a naturally fractured reservoir through discrete fracture networks and homogenized media. *SPE Reservoir evaluation & engineering*, vol. 11, n. 04, pp. 750–758, 2008.

[4] A. Moinfar, A. Varavei, K. Sepehrnoori, and R. T. Johns. Development of an efficient embedded discrete fracture model for 3d compositional reservoir simulation in fractured reservoirs. *SPE Journal*, vol. 19, n. 02, pp. 289–303, 2014.

[5] M. Ţene, S. B. Bosma, M. S. Al Kobaisi, and H. Hajibeygi. Projection-based embedded discrete fracture model (pedfm). *Advances in Water Resources*, vol. 105, pp. 205–216, 2017.

[6] J. Jiang and R. M. Younis. An improved projection-based embedded discrete fracture model (pedfm) for multiphase flow in fractured reservoirs. *Advances in water resources*, vol. 109, pp. 267–289, 2017.

[7] H. U. Rashid and O. Olorode. A continuous projection-based edfm model for flow in fractured reservoirs. *SPE Journal*, vol. 29, n. 01, pp. 476–492, 2024.

[8] Z. Gao and J. Wu. A linearity-preserving cell-centered scheme for the heterogeneous and anisotropic diffusion equations on general meshes. *International Journal for Numerical Methods in Fluids*, vol. 67, n. 12, pp. 2157–2183, 2011.

[9] J. Teixeira, D. Carvalho, T. Cavalcante, K. Angelim, and P. Lyra. Numerical simulation of oil-water displacements in naturally fractured reservoirs using a hybrid grid mpfa-streamline (sls-hyg) formulation. *Computers and Geotechnics*, vol. 151, pp. 104963, 2022.

[10] F. R. Contreras, U. A. Vaz, G. L. Pacheco, A. R. Antunes, P. R. Lyra, and D. K. Carvalho. A high-resolution multidimensional finite volume scheme coupled to a nonlinear two-point flux approximation method for the numerical simulation of groundwater contaminant transport using unstructured 2d meshes. *Advances in Water Resources*, vol. 181, pp. 104559, 2023.

[11] F. R. Contreras, U. A. Vaz, A. R. Antunes, P. R. Lyra, and D. K. Carvalho. A non-linear finite volume method coupled with a higher order muscl-type formulation for the numerical simulation of groundwater solute trans-port. In *XLII Ibero-Latin American Congress on Computational Methods in Engineering*, volume 3, 2021.

[12] T. d. M. Cavalcante, A. C. Souza, H. Hajibeygi, D. K. Carvalho, and P. R. Lyra. Simulation of two-phase flow in 3d fractured reservoirs using a projection-based embedded discrete fracture model on unstructured tetrahedral grids (pedfm-u). *Advances in Water Resources*, vol. 187, pp. 104679, 2024.

[13] X. Rao and Y. Liu. A numerical modelling method of fractured reservoirs with embedded meshes and topological fracture projection configurations. *Comput Model Eng Sci*, vol. 131, n. 3, pp. 1403–1429, 2022.

[14] D. Wu, Y. Di, and Y.-S. Wu. A new projection-based integrally embedded discrete fracture model and its application in coupled flow and geomechanical simulation for fractured reservoirs. *Geofluids*, vol. 2022, n. 1, pp. 7531948, 2022.

[15] E. W. Dijkstra. A note on two problems in connexion with graphs. In *Edsger Wybe Dijkstra: his life, work, and legacy*, pp. 287–290, 2022.